

Enhanced collective stopping and drift of electron beams in fusion plasmas with heavy-ion speciesXiao-Juan Wang , Zhang-Hu Hu,^{*} and You-Nian Wang*School of Physics, Dalian University of Technology, Dalian 116024, People's Republic of China* (Received 24 December 2019; revised manuscript received 19 February 2020; accepted 17 March 2020; published 10 April 2020)

The transport and energy deposition of relativistic electron beams in transversely nonuniform plasmas are investigated with two-dimensional electromagnetic particle-in-cell simulations. For the beam with radius much larger than plasma skin depth, the current filamentation instability excited by the electron beam can be observed, which breaks the beam into filaments and leads to the formation of strong magnetic fields consequently. The effects of plasma ion species are significant and asymmetric transverse magnetic fields are formed in plasmas with heavy-ion species due to the asymmetric neutralization of beam space charge by plasma ions. The asymmetric transverse magnetic fields contribute to the directional drift of beam electrons to lower plasma density regions, which may accelerate the filaments merger process and lead to highly localized beam-energy deposition in plasmas.

DOI: [10.1103/PhysRevE.101.043203](https://doi.org/10.1103/PhysRevE.101.043203)**I. INTRODUCTION**

The transport of high-current electron beams in plasmas is a research topic relevant to many fields of physics, ranging from high-energy-density physics [1,2] to inertial confinement fusion [3–5] and magnetic reconnection [6]. In the fast ignition of inertial confinement fusion, essential energy for the hot-spot ignition can be transported into the compressed plasma fuel with energetic beam electrons. For the beam-plasma system in the relativistic regime, beam transport and energy deposition can be influenced by numerous collective instabilities, such as the two-stream [7,8] and current filamentation instability (CFI) [9–11]. CFI breaks the electron beam with radius much larger than plasma skin depth into a large number of filaments with a typical radius $r \sim c/\omega_{pe}$ and thereby leads to the formation of strong magnetic fields. Subsequently, these filaments merge into denser filaments under the action of the magnetic field. Besides, the merging of the filaments, which is responsible for the magnetic reconnection [6,12], is also an important issue for beam energy deposition.

Considerable research efforts have been devoted to the influence of CFI on the transport and energy deposition of relativistic electron beams traveling through uniform plasmas. During the linear stage of the instability, a strong collective beam energy stopping and an exponential growth of the magnetic field energy were clearly observed. The major dissipative mechanism is originated from filaments merger and subsequent radial dynamics, which is different from binary Coulomb collisions [13]. The super-Alfvénic currents and hollow-current density profiles of the beam filaments in the nonlinear stage of the instability was demonstrated by numerical and analytic results [14,15]. Experimental evidence of CFI in a laboratory setting with accelerator electron beams and capillary discharge plasma was presented [16]. The transition

from multiple filaments to single filament was observed by varying the plasma density. Besides, the merging of these electron filaments is responsible for the stepwise changes of the beam current and the magnetic or particle energies [14,15,17]. Due to the large mass difference, the dynamic effects of plasma ions were shown to be important and have significant impacts on the direction of transverse electric fields [14,18].

In actual experiments, such as the fast ignition, the relativistic electron beams may travel through the plasma with enormous density gradients, from 10^{22} cm^{-3} near the critical surface to 10^{26} cm^{-3} in the dense core where the ignition occurs [14,19]. In addition to the density gradient in the longitudinal direction (i.e., the direction along the beam propagation direction), plasmas may also have density gradient in the transverse direction (i.e., the direction perpendicular to the beam propagation direction). To the present, little attention has been paid to the transport of electron beams in transversely nonuniform plasmas, especially with different ion species. Actually, this is the case in inertial confinement fusion, in which different ablator materials are frequently adopted. It should be noted that, due to low mode asymmetries and increased ablator surface perturbations, the onset of the Rayleigh-Taylor instability is primarily responsible for the mixing of ablator material into the DT hot spot in the central spark ignition. In the fast ignition with cone-in-shell targets, a hollow Au cone is inserted in the spherical shell and the Au ions with lower energies are generated at the cone tip, deep into the hot spot as the heavy-ion composition. In this work, we show that the effects of plasma ion species are significant and can contribute to the directional drift of beam electrons in the transverse direction, which may lead to a highly localized beam energy deposition in plasmas. Bret *et al.* [10,11] systematically investigated the electromagnetic instabilities in the whole k space for the electron beam interacting with transversely uniform plasmas. And the fastest-growing mode for the system is shown to be oblique. In this work,

^{*}zhanghu@dlut.edu.cn

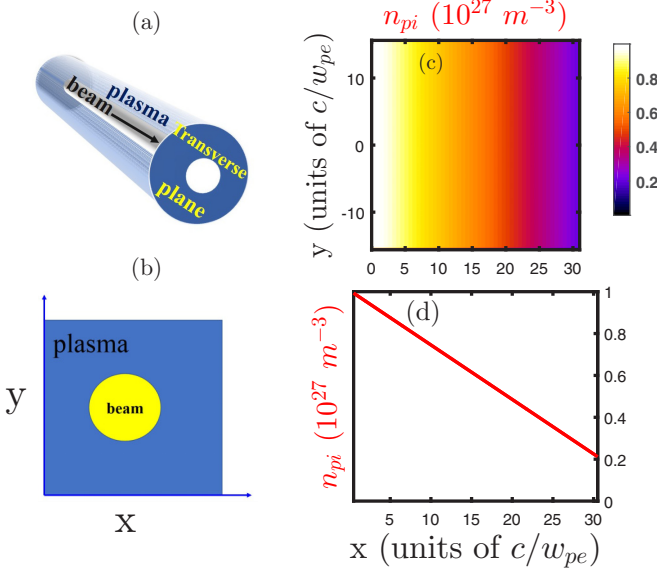


FIG. 1. Schematic of the beam-plasma interaction system (a) and transverse simulation plane (b). Initial distributions of plasma density n_{pi} (c) and corresponding slice distributions of n_{pi} (d) at the position $y = 0$ are also displayed. Here the maximum and minimum plasma density in the x direction are set to be 10^{27} m^{-3} and $2 \times 10^{26} \text{ m}^{-3}$, respectively.

we investigate the transport of relativistic electron beams in transversely nonuniform plasmas and mainly focus on the beam drift in the later stage of CFI. Besides, the two-stream instability is excluded in the simulation with a transverse simulation plane. The paper is organized as follows: In Sec. II the adopted simulation model is described, along with the beam parameters. In Sec. III the formation of asymmetric transverse magnetic fields and the result beam drift are analyzed. Influences of plasma ion species and density gradient are investigated in detail in Sec. IV. Finally, conclusions are given in Sec. V.

II. SIMULATION MODEL

In this work we concentrate on physics and use a simplified model which is two-dimensional (2D) in space (i.e., very long electron beam propagating in the homogeneous z direction [Fig. 1(a)]) and three-dimensional in the plasma and beam momenta. The beam electrons propagate perpendicular to the transverse simulation plane, as indicated in Fig. 1(b). The 2D electromagnetic particle-in-cell (PIC) simulation code IBMP [7,8,18] is adopted here to investigate the transport and energy deposition of relativistic electron beams in plasmas with transversely nonuniform density profiles. In the simulation, the density, temperature, and velocity of the beam electrons are set to be $n_{be} = 10^{26} \text{ m}^{-3}$, $T_b = 1 \text{ keV}$, and $v_{be} = 0.9c$, respectively. Here c is the speed of the light. The initial beam density profile is assumed to be flat-top. Beam electrons are injected into the background plasma with charge neutralization but without current neutralization in the beam edge regions. In the following sections, the beam parameters are kept fixed and the influences of different plasma density profiles and ion species are investigated in detail.

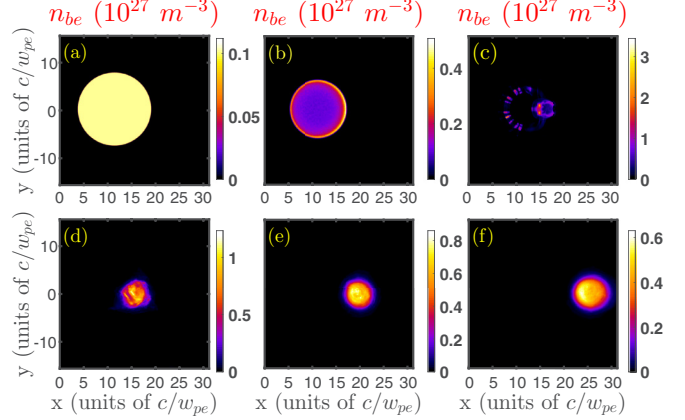


FIG. 2. Density evolutions of the electron beam n_{be} with radius $r_b = 7.6c/\omega_{pe}$ in the linearly distributed Au plasma. Snapshots of six different travel times are shown with (a) $\omega_{pe}t = 0$, (b) $\omega_{pe}t = 40$, (c) $\omega_{pe}t = 40$, (d) $\omega_{pe}t = 112$, (e) $\omega_{pe}t = 202$, and (f) $\omega_{pe}t = 281$.

III. DRIFT OF BEAM ELECTRONS TO LOWER PLASMA DENSITY REGIONS

We first investigate here the electron beam transport in a transversely nonuniform Au plasma. The initial plasma electron temperature is set to be $T_p = 1 \text{ keV}$. The charge state of plasma ions is set to be 1. To simplify the analysis, we suppose that the plasma is linearly distributed in the x direction and uniformly distributed in the y direction. The maximum and minimum plasma density in the x direction are set to be 10^{27} m^{-3} and $2 \times 10^{26} \text{ m}^{-3}$, respectively, as displayed in the Figs. 1(c) and 1(d). In this case, the radius of the electron beam is $r_b = 7.6c/\omega_{pe}$, much larger than plasma skin depth c/ω_{pe} (here ω_{pe} is the plasma electron frequency and is calculated by the maximum density $n_{pe} = 10^{27} \text{ m}^{-3}$). Initially, the center of the electron beam is located at the position $x = 11c/\omega_{pe}$ and $y = 0$. The self-consistent beam structure evolutions at six travel times are shown in Fig. 2. Here the ring structure [7] in the edge regions can also be observed in the transversely nonuniform plasma. One can clearly see that the radius of the electron beam decreases and the density peak near the beam edge increases [Fig. 2(b)]. As the travel time increases, the filamentation of the beam [Fig. 2(c)] [20–22] due to CFI and later merging of the beam filaments into a single one [Fig. 2(d)] can be expected. In the transversely nonuniform plasma, we want to note here some asymmetric effects in the ring structure and beam filamentation [Figs. 2(b) and 2(c)], in which larger filaments are formed in the lower plasma density side. By inspecting Figs. 2(d)–2(f), one can clearly see that the beam obtains a transverse drift velocity and moves to the lower plasma density regions.

To clearly explain the directional drift of the beam, we display the distributions of the electron beam density n_{be} (a), plasma electron density n_{pe} (c), and transverse magnetic field B_y (e) at the travel time $\omega_{pe}t = 198$ in Fig. 3. The corresponding slice distributions of n_{be} , n_{pe} , and $|B_y|$ along the x axis at the position $y = 0$ are also displayed in Figs. 3(b), 3(d) and 3(f), respectively. As indicated in Fig. 3(a), at the selected travel time the filaments have merged into a single one (with only one filament left in the plasma the analysis in the

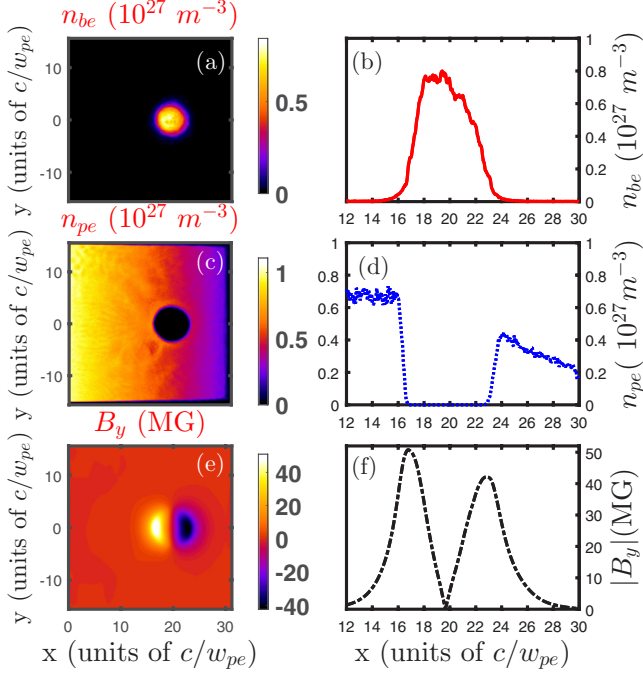


FIG. 3. Distributions of the electron beam density n_{be} (a), plasma electron density n_{pe} (c), and transverse magnetic field B_y (MG) (e) at the travel time $\omega_{pe}t = 198$. The corresponding slice distributions of n_{be} (b), n_{pe} (d), and $|B_y|$ (f) along the x direction at the position $y = 0$ are displayed.

following can be simplified) and the beam density increases significantly, reaching $7 \times 10^{26} \text{ m}^{-3}$ (about 7 times larger than the initial value). Here the beam-plasma interaction is in the nonlinear region with $n_{be} > n_{pe}$. Meanwhile, plasma electrons are expelled from the interior regions of the beam electrons [Figs. 3(c) and 3(d)]. Thus the space charges of the plasma gold ions is significant and play a key role in the later evolution of the beam. Considering that the space charges of the beam electrons are neutralized by that of plasma ions with linearly distributed profile, the un-neutralized beam charges (which are defocusing for beam electrons) on the right side (i.e., lower ion density regions) of the beam are larger, and thus a weaker focusing effect can be expected. Consequently, an asymmetry in the beam density profile along the x direction is induced, as indicated in Fig. 3(b). In the figure, the beam radius on the right side (i.e., lower ion density regions) is about $4c/w_{pe}$, while that on the left side is about $3c/w_{pe}$. For the simulations in the transverse geometry, we concentrate only on the transverse spatial dynamics of the beam-plasma interaction. The leading transverse component of the magnetic field, which lies in the x - y plane, can be expressed as $\vec{B}_\perp = -\vec{e}_z \times \nabla_\perp \psi$, where ψ is the z component of the vector potential. Conservation of the generalized vorticity [23] $\vec{\Omega} \equiv \nabla \times \vec{v}_e - e\vec{B}/m_e$ enables us to give a relation between the z component of plasma electron fluid velocity \vec{v}_e and the vector potential as $v_{ez} = e\psi/m_e$. Projecting Ampere's law, $\nabla \times \vec{B} = \mu_0(\vec{J}_p + \vec{J}_b)$, on the z axis and using $v_{ez} = e\psi/m_e$ yields the equation for the vector potential $\nabla^2 \psi = \frac{\omega_{pe}^2}{c^2} \psi - \mu_0 J_{bz}$. Here in the equation $\vec{J}_b = -en_{be}\vec{v}_b$ and $\vec{J}_p = -en_p\vec{v}_p$ are beam and plasma electron currents, respectively, and the displacement

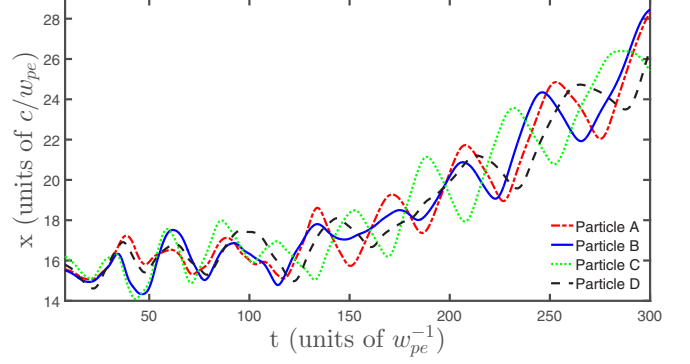


FIG. 4. The trajectories of four random selected beam electrons along the x direction.

current is neglected. With $B_y = -\frac{\partial \psi}{\partial x}$ and $v_{bz} \approx c$, an equation for B_y can be obtained as

$$\nabla^2 B_y = \frac{\omega_{pe}^2}{c^2} B_y - ec\mu_0 \frac{\partial n_{be}}{\partial x}. \quad (1)$$

The solution to Eq. (1) is given by

$$B_y(\vec{x}_\perp) = ec\mu_0 \int G(\vec{x}_\perp - \vec{x}'_\perp) \frac{\partial n_{be}}{\partial x} d^2 x'_\perp, \quad (2)$$

where $G(\vec{x}_\perp - \vec{x}'_\perp) \equiv iH_0^{(1)}(i\frac{\omega_{pe}}{c}|\vec{x}_\perp - \vec{x}'_\perp|)/4$ is the Green's function, $H_0^{(1)}$ is the Hankel function of the first kind and order zero, and the integration is performed over the entire transverse plane. Equation (2) therefore implies the dependence of B_y profile on the source $\frac{\partial n_{be}}{\partial x}$. From Fig. 3(b), the term $\frac{\partial n_{be}}{\partial x}$ (i.e., the slope of beam profile) on the left side is relatively larger than that on the right side. Therefore the formation of the asymmetric magnetic field along the x direction can be expected. The peak magnitudes of the transverse magnetic field in the high- and low-plasma-ion-density regions are shown to be 50 and 40 MG, respectively [Fig. 3(f)]. For beam electrons, the magnitude of magnetic force is significant larger than that of electric force, which is not shown here.

Figure 4 shows the trajectories of four random selected beam electrons (marked as A, B, C, and D). First, the betatron oscillation of beam electrons due to the magnetic force can be clearly observed. At the same time, the amplitude of electron betatron oscillation is smaller in the higher-ion density side and vice versa due to the magnetic field asymmetry, leading to the drift of beam electrons to the lower-plasma-density regions, as clearly indicated in the figure. As the beam electrons interact self-consistently with the asymmetric magnetic field, the directional drift of the beam to the lower-plasma-density regions can thus be expected. Furthermore, as the drift time increases, the un-neutralized beam space charges increase and the decrease of the beam density can thus be expected [comparing Figs. 2(d)–2(f)], which further leads to the decrease of longitudinal beam current density and thus the transverse magnetic field. As a result, the amplitude and period of the betatron oscillations increase as beam electrons moving to lower density regions, which can be clearly identified in Fig. 4 with increasing travel time.

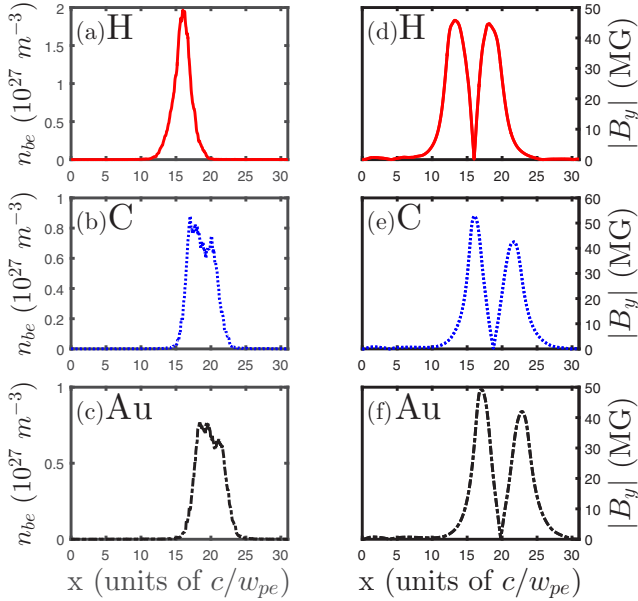


FIG. 5. Slice distributions of the beam electron density n_{be} [(a)–(c)] and transverse magnetic field $|B_y|$ [(d)–(f)] along the x direction at the position $y = 0$ for the H-, C-, and Au-plasma cases. The travel time in the figure is $\omega_{pe}t = 202$.

IV. EFFECTS OF PLASMA ION SPECIES AND DENSITY GRADIENT

We further investigate here the transport of beam electrons in plasmas with different ion species. Three cases are considered here: the hydrogen-, carbon-, and gold-plasmas, which are frequently encountered in inertial confinement fusion. For simplicity, the charge state of plasma ions is assumed to be one for all three cases. The plasma density profile and beam parameters are the same as described in Sec. II. Slice distributions of beam electron density n_{be} [Figs. 5(a)–5(c)] and transverse magnetic field $|B_y|$ [Figs. 5(d)–5(f)] along the x direction at the position $y = 0$ for H-, C-, and Au-plasma cases are displayed in Fig. 5. The density distributions of plasma electrons n_{pe} [Fig. 6(a)–6(c)] and plasma ions n_{pi} [Fig. 6(d)–6(f)] for three plasma cases are also shown in Fig. 6. Due to the defocusing effect of the magnetic field, the plasma electrons are expelled from the beam regions [Figs. 6(a)–6(c)]. For hydrogen plasma, the protons can respond effectively to the beam field and the space charge of beam electrons can be effectively neutralized. As indicated in Fig. 6(d), a high density spot of the proton is formed at the position of beam center and the plasma ions in this case can be considered to be movable. Furthermore, the degrees of beam space charge neutralization by plasma ions are comparable now along the x direction, leading to a symmetric beam density profile [Fig. 5(a)]. From Fig. 5(d), the asymmetric effect in the transverse magnetic field B_y is small and the magnitude of two field peaks in the high- and low-plasma-density regions are comparable. After the filaments merging into a single one, the beam is trapped without any directional drift in the transverse direction.

While for the plasmas with heavy-ion species, the ions cannot respond to the beam field and are provided as the

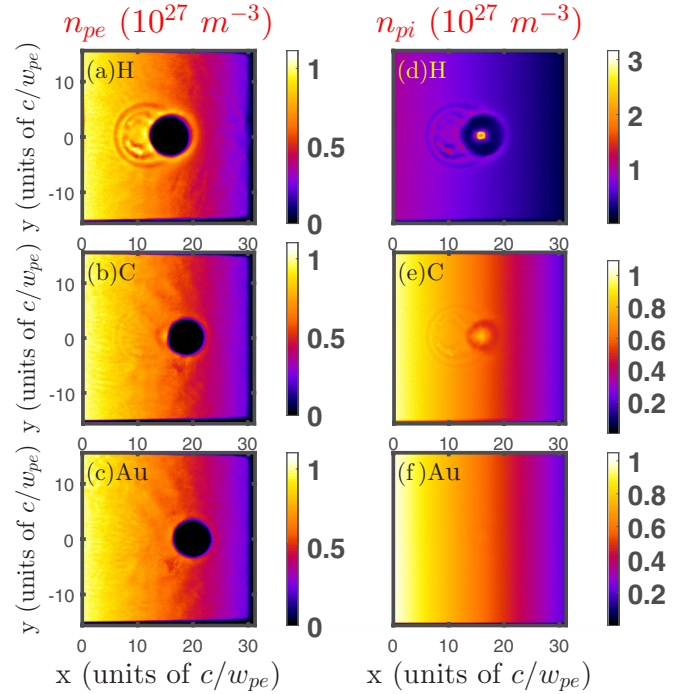


FIG. 6. Distributions of plasma electron density n_{pe} [(a)–(c)] and ion density n_{pi} [(d)–(f)] for the H-, C-, and Au-plasma cases. The beam travel time is the same as in Fig. 5.

charge neutralization background. Due to the ion density gradient, the degree of beam charge neutralization is smaller in the lower density side, leading to a weaker beam focusing effect and lower beam density. Therefore the asymmetry in the beam profile is formed, as explained in Sec. III. From Fig. 6(f), one can clearly see that the ions of the Au-plasma can be considered to be immovable. For both C- and Au-plasmas, the drift of beam electrons to lower plasma density regions [Figs. 5(b) and 5(c)] and asymmetric transverse magnetic field formation can be clearly observed. From Figs. 5(e) and 5(f), the difference in the magnitudes of two magnetic field peaks in high- and low-plasma-density sides is about 10 MG.

Finally, we consider here the beam evolutions in C-plasmas with different linear density gradients. Here the maximum plasma density in the x direction is assumed to be 10^{27} m^{-3} . The minimum plasma densities are set to be 10^{27} m^{-3} (case I), $5 \times 10^{26} \text{ m}^{-3}$ (case II), and $2 \times 10^{26} \text{ m}^{-3}$ (case III). For case I, the plasma is uniform and thus the transverse magnetic field is symmetric about the beam axis [Fig. 7(d)]. In this case, the beam center stays near the initial position, i.e., $x \approx 12c/\omega_{pe}$ and $y = 0$. As the plasma density gradient increases, the asymmetry in the beam space charge neutralization increases and thus the transverse magnetic field [Figs. 7(e) and 7(f)], leading to a more significant beam drift to lower density regions.

Further simulations are performed here to show the transport and energy deposition of electron beams in C-plasmas with more realistic transverse density profiles. Three cases are evaluated here, as indicated in Figs. 8(g)–8(i), in which the distributions of plasma ion density n_{pi} for the exponential decay (case I), uniform (case II), and hollow channel (case III) cases are displayed. In all three cases, the plasma density

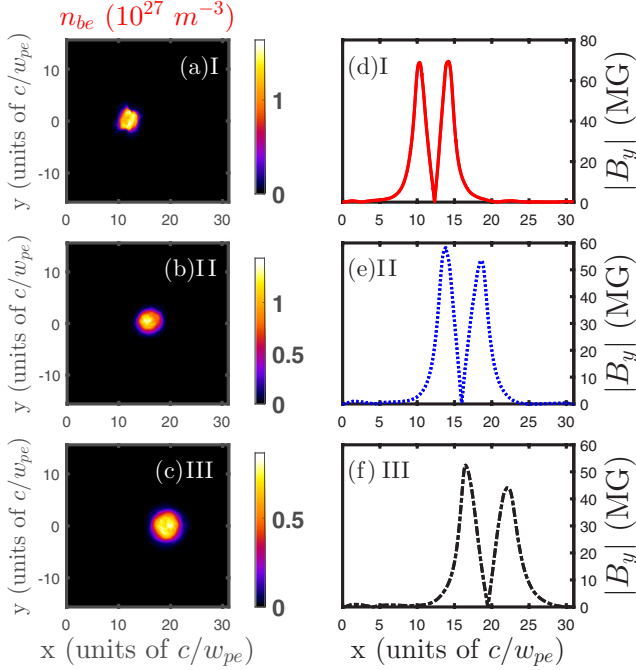


FIG. 7. Distributions of the beam density n_{be} [(a)–(c)] and slice distributions of the transverse magnetic field $|B_y|$ [(d)–(f)] at the position $y = 0$ for different plasma density gradients. Here the maximum plasma density in the x direction is set to be 10^{27} m^{-3} . The minimum plasma densities are set to be 10^{27} m^{-3} (case I), $5 \times 10^{26} \text{ m}^{-3}$ (case II), and $2 \times 10^{26} \text{ m}^{-3}$ (case III). The travel time in the figure is $\omega_{pe}t = 216$.

is azimuthal symmetric. We also show the initial radial slice distributions of n_{pi} at the position $y = 0$ in Fig. 9(a). Here the maximum density of case I, density of case II, and minimum density of case III are set to be 10^{27} m^{-3} . Note that the electron beam are located at the center of the simulation region initially.

As discussed above, in the nonuniform plasma cases, the beam electrons can obtain a transverse drift velocity due to the asymmetric magnetic field and move to lower-plasma-density regions. Therefore, one can expect that during the merger process, beam filaments also obtain a radial drift velocity and move toward the simulation boundary for case I, while toward the center for case III. This drift velocity shows important impacts on the later stage of beam filament merger process. Especially for case III, the drift velocity toward the center can accelerate the merger process effectively. As indicated in Fig. 8(c), there is only one single filament left in the plasma at the selected time. While there are still two filaments in the uniform plasma [Fig. 8(b)] and four in the case I [Fig. 8(a)]. As indicated in previous work [13], the merger process is always associated with a strong collective stopping of beam electrons, converting the beam energy to the magnetic field energy and plasma kinetic energy. Comparing the beam energy evolution for three plasma cases in Fig. 9(b), one can clearly see that for case III the beam can deposit significant energy in a shorter time than cases I and II, due to the acceleration of merger process by the radial drift velocity. From the solid line of Fig. 9(b), a highly localized beam

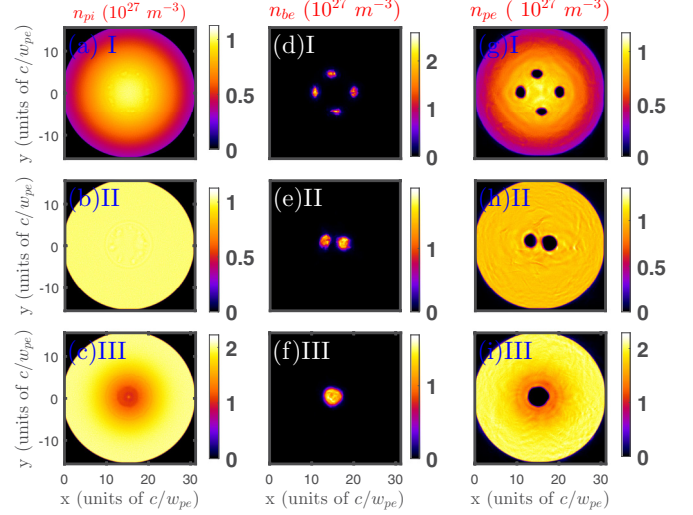


FIG. 8. Distributions of beam density n_{be} [(a)–(c)], plasma electron density n_{pe} [(d)–(f)], and plasma ion density n_{pi} [(g)–(i)] for the plasmas with exponential decay [case I: (a), (d), and (g)], uniform [case II: (b), (e), and (h)], and hollow channel [case III: (c), (f), and (i)] density cases. The travel time in the figure is $\omega_{pe}t = 90$ for three density cases.

energy deposition can be clearly observed near the travel time $50/\omega_{pe}$. The beam electrons are seen to deposit half of its initial kinetic energy within a travel time of $60/\omega_{pe}$. Deutsch *et al.* [5] have shown that the energy loss of beam electrons occurs essentially as classical stopping due to the large value of $n_p/n_b \sim 10^5$ at core density. In this work, for the hollow channel case in Fig. 8 with $n_p/n_b \sim 10$, the beam electrons are seen to deposit half of its initial kinetic energy (about 0.4 MeV) within a travel time of $60/\omega_{pe}$, corresponding to 34 fs and a beam propagation distance of $v_{be}t = 9.2 \text{ } \mu\text{m}$. With these information, we find effective stopping powers a factor of 100–1000 larger than due to classical stopping involving electron-electron collision and collective Langmuir contributions.

V. CONCLUSION

Beam-plasma interaction is one of the most promising applications in plasma physics for science and commerce. In

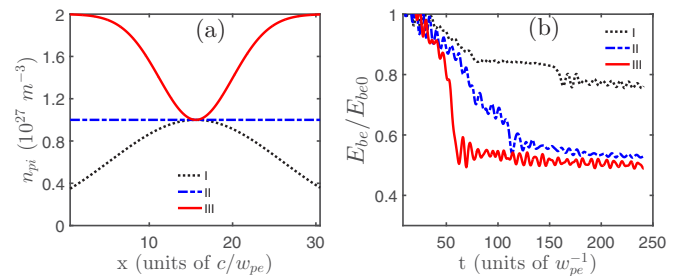


FIG. 9. (a) Radial slice distributions of the plasma ion density n_{pi} at the position $y = 0$ and (b) time evolution of the electron beam kinetic energy E_{be} (normalized by E_{be0}) for three plasma density cases. Here E_{be0} is initial kinetic energies of the electron beam.

the actual experiments, the high-current electron beam may travel through plasmas with density gradient both in directions parallel and perpendicular to the beam propagation direction. Besides, the interaction of high-current beam with plasmas of different ion species are frequently encountered, such as in inertial confinement fusion, in which different ablator materials are frequently used. The CFI stands as a key process in intense electron beam-plasma interactions. The resulting magnetic fields may grow strong enough to cause significant scattering and deceleration of the beam electrons. In this work, the transport of the electron beam traveling through the transversely nonuniform plasmas are investigated in detail with PIC simulations. It is shown that strong asymmetric transverse magnetic fields are formed in plasmas with heavy-ion species

due to the asymmetric neutralization of beam space charge by plasma ions. The asymmetric transverse magnetic fields contribute to the directional drift of beam electrons to lower plasma density regions, which may accelerate the filaments merger process and lead to a highly localized beam energy deposition in plasmas. These effects are detrimental to the fast ignition of inertial confinement fusion.

ACKNOWLEDGMENTS

This work is supported by the National Natural Science Foundation of China (Projects No. 11775042 and No. U1532263) and the Fundamental Research Funds for the Central Universities (Grant No. DUT18TD06).

-
- [1] R. P. Drake, *High-Energy-Density Physics* (Springer-Verlag, Berlin, 2006).
 - [2] N. A. Tahir, D. H. H. Hoffmann, A. Kozyreva, A. Shutov, J. A. Maruhn, U. Neuner, A. Tauschwitz, P. Spiller, and R. Bock, Shock compression of condensed matter using intense beams of energetic heavy ions, *Phys. Rev. E* **61**, 1975 (2000).
 - [3] M. Tabak, J. Hammer, M. E. Glinsky, W. L. Kruer, S. C. Wilks, J. Woodworth, E. M. Campbell, M. D. Perry, and R. J. Mason, Ignition and high gain with ultrapowerful lasers, *Phys. Plasmas* **1**, 1626 (1994).
 - [4] M. Tabak, D. S. Clark, S. P. Hatchett, M. H. Key, B. F. Lasinski, R. A. Snavely, S. C. Wilks, R. P. J. Town, R. Stephens, E. M. Campbell, R. Kodama, K. Mima, K. A. Tanaka, S. Atzeni, and R. Freeman, Review of progress in fast ignition, *Phys. Plasmas* **12**, 057305 (2005).
 - [5] C. Deutsch, H. Furukawa, K. Mima, M. Murakami, and K. Nishihara, Interaction Physics of the Fast Ignitor Concept, *Phys. Rev. Lett.* **77**, 2483 (1996).
 - [6] S. R. Titorica, T. Abel, and F. Fiuza, Nonthermal Electron Energization from Magnetic Reconnection in Laser-Driven Plasmas, *Phys. Rev. Lett.* **116**, 095003 (2016).
 - [7] Z. H. Hu, X. J. Wang, Y. T. Zhao, and Y. N. Wang, Double-ring structure formation of intense ion beams with finite radius in a pre-formed plasma, *Phys. Plasmas* **24**, 123103 (2017).
 - [8] Z. H. Hu and Y. N. Wang, Hollow structure formation of intense ion beams with sharp edge in background plasmas, *Phys. Plasmas* **23**, 023103 (2016).
 - [9] E. S. Weibel, Spontaneously Growing Transverse Waves in a Plasma Due to an Anisotropic Velocity Distribution, *Phys. Rev. Lett.* **2**, 83 (1959).
 - [10] A. Bret, M.-C. Firpo, and C. Deutsch, Characterization of the Initial Filamentation of a Relativistic Electron Beam Passing through a Plasma, *Phys. Rev. Lett.* **94**, 115002 (2005)
 - [11] A. Bret, M.-C. Firpo, and C. Deutsch, Collective electromagnetic modes for beam-plasma interaction in the whole k space, *Phys. Rev. E* **70**, 046401 (2004).
 - [12] J. T. Dahlin, J. F. Drake, and M. Swisdak, The mechanisms of electron heating and acceleration during magnetic reconnection, *Phys. Plasmas* **21**, 092304 (2014).
 - [13] M. Honda, J. Meyer-ter-Vehn, and A. Pukhov, Collective Stopping and Ion Heating in Relativistic-Electron-Beam Transport for Fast Ignition, *Phys. Rev. Lett.* **85**, 2128 (2000).
 - [14] G. Shvets, O. Polomarov, V. Khudik, C. Siemon, and I. D. Kaganovich, Nonlinear evolution of the Weibel instability of relativistic electron beams, *Phys. Plasmas* **16**, 056303 (2009).
 - [15] O. Polomarov, I. D. Kaganovich, and G. Shvets, Merging of Super-Alfvenic Current Filaments During Collisionless Weibel Instability of Relativistic Electron Beams, *Phys. Rev. Lett.* **101**, 175001 (2008).
 - [16] B. Allen, V. Yakimenko, M. Babzien, M. Fedurin, K. Kusche, and P. Muggli, Experimental Study of Current Filamentation Instability, *Phys. Rev. Lett.* **109**, 185007 (2012).
 - [17] C. Shukla, A. Kumar, A. Das, and B. G. Patel, Merger and reconnection of Weibel separated relativistic electron beam, *Phys. Plasmas* **25**, 022123 (2018).
 - [18] X. J. Wang, Z. H. Hu, Y. T. Zhao, and Y. N. Wang, Modulation of proton beams by relativistic electron beam-plasma instability, *Phys. Plasmas* **25**, 102104 (2018).
 - [19] J. J. Honrubia and J. Meyer-ter-Vehn, Three-dimensional fast electron transport for ignition-scale inertial fusion capsules, *Nucl. Fusion* **46**, L25 (2006).
 - [20] T. Taguchi, T. M. Antonsen, Jr., C. S. Liu, and K. Mima, Structure Formation and Tearing of an MeV Cylindrical Electron Beam in a Laser-Produced Plasma, *Phys. Rev. Lett.* **86**, 5055 (2001).
 - [21] M. C. Firpo, A. F. Lifschitz, E. Lefebvre, and C. Deutsch, Early Out-of-Equilibrium Beam-Plasma Evolution, *Phys. Rev. Lett.* **96**, 115004 (2006).
 - [22] Z. H. Hu, X. J. Wang, T. L. Shang, and Y. N. Wang, Longitudinal magnetic field generation during the early stage of relativistic electron beam-plasma interaction, *Phys. Plasmas* **26**, 073104 (2019).
 - [23] I. D. Kaganovich, G. Shvets, E. Startsev, and R. C. Davidson, Nonlinear charge and current neutralization of an ion beam pulse in a pre-formed plasma, *Phys. Plasmas* **8**, 4180 (2001).